R-matrix calculations for electron-impact excitation of C^+, N^{2+}, and O^{3+} including fine structure

D. Luo and A. K. Pradhan*
Joint Institute for Laboratory Astrophysics, University of Colorado and National Institute of Standards and Technology, Boulder, Colorado 80309-0440
(Received 5 July 1989)

Close-coupling calculations are carried out using the R-matrix method for the excitation of a number of states of boronlike carbon, nitrogen, and oxygen by electron impact. The ten lowest LS states of C^+ and the eight lowest states of N^{2+} and O^{3+} are considered in the eigenfunction expansions. Including fine structure the collision strengths are calculated for all transitions among the states $2s^22p(^2P^o_{1/2,3/2})$, $2s2p^2(^4P_{1/2,3/2,5/2},^2D_{3/2,5/2},^2S_{1/2},^2P_{1/2,3/2})$, $2p^3(^4S^o_{3/2},^2D^o_{3/2,5/2},^2P^o_{1/2,3/2})$, $2s^23s(^2S_{1/2})$, and $2s^23p(^2P^o_{1/2,3/2})$ for C^+ and among all states of N^{2+} and O^{3+} excluding the $n=3$ configurations. Resonance structures in the collision strengths are delineated at a large number of energies and are found to have a substantial effect. A number of selected results are presented, in particular for the fine-structure transition $^2P^o_{1/2}$-$^2P^o_{3/2}$ and the resonance transition $^2P^o$-^2D in all three ions.

I. INTRODUCTION

The R-matrix method has proved to be very successful for an accurate and extensive treatment of a variety of atomic processes, both radiative and collisional.[1] In the past five or six years the radiative applications have received particular attention in order to calculate stellar opacities with state-of-the-art atomic physics.[2] The radiative work has involved extensive calculations for the oscillator strengths and photoionization cross sections for all astrophysically abundant elements and their ions. The R-matrix method, initially developed by Burke *et al.* (see Ref. 1), has been considerably extended and modified for more optimal computations for radiative and collisional work. In the present report we have applied the new R-matrix package for comprehensive close-coupling calculations for electron scattering with the first three ions in the boron isoelectronic sequence: C^+, N^{2+}, and O^{3+}. A prime motivation for the selection of these ions is their considerable astrophysical significance. Other important reasons for their study are that experimental measurements may soon be available for absolute cross sections for several transitions in C^+ (one set of measurements is already available), and that a few previous calculations have been carried out by other workers for all three ions.

The collision strengths have been calculated in the LS coupling approximation, as well as in a pair-coupling scheme, for the transitions among the fine-structure sublevels. Calculations are carried out at a large number of energies in order to study the detailed effects of autoionizing resonances.

II. THEORY

The close-coupling method entails a numerically exact solution of the many electron Schrödinger equation for the electron + ion system, subject to the constraint that a finite (usually small) number of ionic states are included in the eigenfunction expansion. For each $SL\pi$ the total (electron + ion) wave function is represented as

$$\Psi(E)=\mathcal{A}\left[\sum_{i=1}^{N}\chi_i\theta_i+\sum_{j=1}^{M}c_j\Phi_j\right], \tag{1}$$

where E is the total energy, χ_i are the ion (target) states, the θ_i represent the free electron, N is the number of channels corresponding to the given eigenstates of the ion, and $\mathcal{A}$ is the antisymmetrization operator. The second term on the right-hand side (rhs) includes (electron + ion) bound-state wave functions, referred to as bound channels, which are included to satisfy orthogonality constraints on the free-electron and the bound-electron orbitals and also to include additional short-range correlation; the c_j are variational coefficients and M is the number of bound-channel terms.

The bound-channel term in Eq. (1) often plays an important role in the proper representation of the total electron-electron correlation in the problem. The number of such terms is essentially arbitrary. However, in practice one includes all such Φ_j functions that can be constructed from the various combinations of the ionic states and the free electron (i.e., from their associated spin and orbital angular momenta). Thus, typically there are a large number of bound-channel terms included in the close-coupling calculations. However, the individual Φ_j functions may not all be represented equally well, in particular if they correspond to the so-called correlation configurations, which in some instances may include pseudo-orbitals (scaled to provide suitable correlation for the primary target, ion terms χ_i). In cases where a large amount of e-e correlation is needed, the number of bound-channel functions is quite large and some of the states may appear at incorrect energies giving rise to pseudoresonances in the cross sections. Usually, however, the pseudostates lie fairly high in energy, relative to the ion threshold energies, and one may remove the effect

of these in one of several ways as we shall describe later.

The $\underline{R}$-matrix method for the solution of the close-coupling equations involves dividing up the configuration space into inner and outer regions, where the inner region envelops the target atom or ion, i.e., the bound-orbital functions of the ion decay down exponentially to negligible values at the boundary of the $\underline{R}$ matrix. In the outer region the wave function is described by the asymptotic behavior of the free electron in the various channels, i.e., by the Coulomb phase plus the phase due to other detailed electron-ion interactions. New, more efficient, asymptotic routines have been developed and incorporated in the extended $\underline{R}$-matrix package (Ref. 1).

The $\underline{R}$-matrix solutions, in LS coupling, for the basis functions to represent the total wave function $\Psi(E)$ are obtained upon diagonalization of the electron + ion Hamiltonian for each total symmetry, i.e., total spin and angular momenta, $SL\pi$ where $\mathbf{S}=\mathbf{S}_i\pm\frac{1}{2}$, $\mathbf{L}=\mathbf{L}_i\pm\mathbf{l}_i$, and $\pi=(-1)^{\sum_i l_i}$; the $\mathbf{S}_i$ and $\mathbf{L}_i$ refer to the target states of the ion, l_i to the orbital angular momentum of the free electron, and π is the parity of the whole system.

In order to treat the fine-structure transitions, one may further make an algebraic transformation from the LS to a pair-coupling scheme,

$$\mathbf{S}_i+\mathbf{L}_i=\mathbf{J}_i;\quad \mathbf{J}_i+\mathbf{l}_i=\mathbf{K}_i;\quad \mathbf{K}_i\pm\tfrac{1}{2}=\mathbf{J}\ .$$

The set of reactance matrices $\{\underline{K}^{SL\pi}\}$ is transformed to $\{\underline{K}^{J\pi}\}$ as (the symbol for the reactance matrix is not to be confused with the one for the angular momentum)

$$\begin{aligned}K^{J\pi}(\Gamma_i J_i l_i K_i,\Gamma_i' J_i' l_i' K_i';E)&=\sum_{S,L,\pi} C(SLJ,S_iL_iJ_i;l_iK_i)\\&\times K^{SL\pi}(\Gamma_i l_i s_i,\Gamma_i' l_i' s_i';E)\\&\times C(SLJ,S_i'L_i'J_i';l_i'K_i')\ ,\end{aligned}$$

where the recoupling coefficients C are given by

$$\begin{aligned}C(SLJ,S_iL_iJ_i,l_iK_i)&=W(Ll_iS_iJ_i;L_iK)W(LJS_is_i;SK)\\&\times[(2S+1)(2L+1)(2K_i+1)\\&\times(2J_i+1)]^{1/2}\ ,\end{aligned}\tag{2}$$

where W is the Racah coefficient (Γ_i refers to the target terms).

The collision strengths may be calculated from the $\underline{T}$ matrix

$$\underline{T}=\underline{1}-\underline{S}=2i\underline{K}(1-i\underline{K})^{-1}\ ,$$

where $\underline{S}$ is the scattering matrix. Further details are described by Saraph.[3] The formulation may also be extended to incorporate quantum-defect theory as given by Seaton,[4] in particular to include a procedure to average over autoionizing resonance structures, referred to as Gailitis averaging (see, for example, Pradhan[5]).

An alternative formulation that leads to numerically more convenient and exact results is to apply the pair-coupling transformation (2) to the $\underline{T}$ matrix rather than the $\underline{K}$ matrix. The advantages of this approach are that (a) the unitarity condition is satisfied more precisely, leading to numerically more exact values; for example, all partial fine-structure collision strengths for transitions among the fine-structure sublevels between two LS terms add up exactly to the LS collision strength; (b) the matrix computations are simplified since the $\underline{T}$ matrix is initially obtained in LS coupling with considerably fewer channels than in pair coupling; and finally, (c) the branching ratios for the fine structure to multiplet collision strengths

$$\frac{\Omega(\Gamma_i S_i L_i J_i-\Gamma_{i'}S_{i'}L_{i'}J_{i'})}{\Omega(\Gamma_i S_i L_i-\Gamma_{i'}S_{i'}L_{i'})}\ ,\tag{3}$$

for cases when either the total $S=0$ or total $L=0$ is numerically closer to the exact value

$$(2J_{i'}+1)/[(2S_{i'}+1)(2L_{i'}+1)]\ .$$

In the present work the calculations were carried out using both the $\underline{K}$-matrix and the $\underline{T}$-matrix formulations and the latter was eventually adopted due to the reasons given. For some other applications, such as the detailed analysis of pole positions and residues of the resonances, it might be more desirable to employ the $\underline{K}$ matrices as they have the advantage of being real and symmetric.

An advantage of interfacing the pair-coupling formulation with the $\underline{R}$-matrix method, not considered in earlier works, is that the fine-structure collision strengths can be obtained at a large number of energies where the LS coupling calculations are carried out.

III. COMPUTATIONS

A. Target states

The accuracy of the close-coupling calculations depends critically on the representation of the target states wave functions χ_i in Eq. (1). Configuration-interaction-type (CI) wave functions are obtained for the χ_i by carrying out a number of atomic structure calculations for the target ion. These calculations for the boron sequence ions are described in detail by Luo and Pradhan[6] who considered the radiative problem for a number of carbon-like ions, within the same formulation and the same target data, and calculated a larger number of oscillator strengths and photoionization cross sections.

In Table I we give the calculated energy levels for C^+, N^{2+}, and O^{3+} and compare these with the experimental values. For C^+ we include ten LS states; the $2s^2 3s\,(^2S)$ and the $2s^2 3p\,(^2P^o)$ lie between other states of the $n=2$ complex and were therefore also considered. However, for N^{2+} and O^{3+} the $n=3$ states are more clearly separated from the $n=2$ states and were excluded.

The CI expansion required for an accurate representation of C^+ states was considerably larger than that for N^{2+} and O^{3+}—23 configurations for C^+ as opposed to 13 for the other two.

B. Electron + ion symmetries

The spin and angular momentum of the target states S_iL_i for the three ions are $^2P^o$, ^4P, ^2D, ^2S, ^2P, $^4S^o$, $^2D^o$.

TABLE I. Energy levels of C^+, N^{2+}, and O^{3+} (in rydbergs).

State	C^+		N^{2+}		O^{3+}	
	E(expt)	E(calc)	E(expt)	E(calc)	E(expt)	E(calc)
$2s^22p(^2P^o)$	0.0000	0.0000	0.0000	0.0000	0.0000	0.0000
$2s2p^2(^4P)$	0.3918	0.3790	0.5209	0.5020	0.6482	0.6291
$2s2p^2(^2D)$	0.6824	0.6917	0.9196	0.9280	1.1545	1.1619
$2s2p^2(^2S)$	0.8789	0.9011	1.1927	1.2212	1.4955	1.5192
$2s2p^2(^2P)$	1.0080	1.0284	1.3289	1.3516	1.6438	1.6659
$2s^23s(^2S)$	1.0616	1.0679				
$2s^23p(^2P^o)$	1.2000	1.2060				
$2p^3(^4S^o)$	1.2939	1.3244	1.7012	1.7196	2.1052	2.1240
$2p^3(^2D^o)$	1.3708	1.4006	1.8505	1.8791	2.3230	2.3517
$2p^3(^2P^o)$	1.5373	1.5785	2.0986	2.1804	2.6315	2.7090

With the incident partial waves truncated at $l_i \leq 6$ we obtain the following total symmetries $SL\pi$ where $\mathbf{S}=\mathbf{S}_i\pm\frac{1}{2}$,

$$\mathbf{L}=\mathbf{L}_i\pm\boldsymbol{l}_i \text{ and } \pi=(-1)^{\sum_i l_i} ,$$

$$^{1,3}(S,P,D,F,G,H,I)^{e,o} ,$$

and

$$^5(S,P,D,F,G)^{e,o} ,$$

for a total of 38 $SL\pi$ states; the e and o refer to even and odd parities.

It might be noted that not all of the quintet symmetries are required for the transitions between the ^4P and the $^4S^o$ states in LS coupling; however, such $SL\pi$'s are still needed for the pair-coupling transformation given by Eq. (2).

The ten-state C^+ calculations were carried out with the number of symmetries given above. For N^{2+} and O^{3+} however, we employed an eight-state target and considered a much larger set of $SL\pi$ states:[1,3,5] $(L=0,12)^{e,o}$; this enabled a partial wave summation up to $l_i \leq 10$.

C. Top-up for allowed transitions

The electron + ion $SL\pi$ states given in Sec. III B refer to partial waves with $l \leq 4$. While for the forbidden transitions this summation should be adequate, for optically allowed transitions one needs to include much higher partial waves. The usual practice in the past has been to complete the partial wave summation for the allowed transition employing the Coulomb-Bethe approximation,[7] in conjunction with the close-coupling calculations.[8] However this approach is not very precise in that one does not exactly obtain a match between the total angular momenta states L, the incident angular momentum l, and the l values included in the Coulomb-Bethe summation. The problem is significantly more exacerbated when the pair-coupling transformation is made and it is required to complete the summation for the optically allowed fine-structure transitions.

Burke and Seaton[9] have recently developed a procedure to "topup" the partial wave summation of collision strengths for allowed transitions in LS coupling taking account of the matching required between the total L and l values included in the $\underline{R}$-matrix calculations. For the LS calculations reported in the present work we have utilized the top-up procedure and the allowed transitions have been summed over for all incident l values.

D. Energy mesh

The energy mesh is chosen so as to delineate the resonance structures with a high degree of resolution. As the autoionization width decreases as n^{-3}, the resonances become narrower and therefore a mesh with a constant energy interval would rapidly lose revolution even for fairly low n states. It is thus preferable to establish a mesh determined by a constant interval in the effective quantum number in order to enable the same resolution for all the resonances to be considered. In addition, the mesh should reflect the convergence of the Rydberg series of resonances on to the target thresholds included in the eigenfunction expansion.

Employing the relation

$$\mathcal{E}=E_i-\frac{z^2}{\nu_i^2} , \tag{4}$$

where $\mathcal{E}$ is the energy variable in the region below the threshold at energy E_i and corresponds to the effective quantum number ν_i calculated relative to E_i. For example, we may choose $\Delta\nu_i=0.025$, with $\nu_i \leq \nu_{\max}$; all resonances up to $\nu_{\max}$ are then resolved with approximately 40 points in each interval where ν_i changes by unity. If $\nu_{\max}$ is taken to be 10, then this corresponds approximately to resonances with $n \leq 10$. The mesh interval is different for different ions and some experimentation is needed to determine the optimum parameters.

In the region just below the convergence of a resonance series limit (i.e., near the corresponding target state), the resonances are very narrow and it is impractical to resolve the resonance structures in detail. We employ the quantum-defect theory averaging procedure due to Gailitis (see Ref. 5) in the region just below each threshold. A special feature of the method incorporated in the present work is that while we obtain the resonance averaged values for the resonances belonging to a given threshold, the resonance structures due to the higher thresholds are not affected. This is necessary since the latter correspond to low-n values and are usually broad. In Sec. III E some examples are given of the detailed and the averaged cross

sections and associated resonances. In general the choice of an energy mesh depends on the problem under consideration and both the constant ΔE or the $\Delta\nu$ types of mesh may need to be employed.

E. Scattering calculations

The new $\underline{R}$-matrix package for electron-ion scattering calculations consists of several stages of separate codes, preceded by the atomic structure codes CIV3 or SUPERSTRUCTURE (Ref. 1). The target CI calculations are carried out using either of these codes and the set of one-electron orbitals are input to the first stage STG1 which calculates the radial matrix elements required to represent the target states. The second stage STG2 is employed to calculate the necessary algebraic coefficients in order to set up the electron-ion Hamiltonian matrix, and to carry out the matrix diagonalization, in the third stage STGH. The $\underline{R}$-matrix obtained in STGH is input to a continuum electron code STGF which calculates the asymptotic electron wave functions, at the chosen mesh of energies, and the collision strengths. The top-up procedure for the allowed transitions is also implemented in STGF. The pair-coupling transformation is carried at a subsequent stage, with input from STGF in the form of the reactance matrices at all energies and all the total $SL\pi$ states necessary to complete the transformation.

IV. RESULTS AND DISCUSSION

Collision strengths were calculated for all 45 inelastic transitions among the ten states of C^+ and 28 transitions among the eight target states of N^{2+} and O^{3+}. In addition, fine-structure collision strengths were also obtained for transitions between all fine-structure substates. The algebraic transformation from the LS to pair-coupling scheme employed in the present work neglects the fine-structure energy differences for the term splittings in the target states, which are assumed much smaller than the LS term differences.

The lowest few transitions in boronlike ions are between the states $2s^22p(^2P^o)\rightarrow 2s2p^2(^4P,^2D,^2S,^2P)$. The first transition from the ground state to the quartet state is spin forbidden but the next three transitions to the doublet states are optically allowed. The three states ^2D, ^2S, and ^2P lie relatively close together and it is expected that the coupling between transitions to these states should be strong. Based on a comparison of the oscillator strengths for transitions from the ground state $^2P^o$, one would expect the $^2P^o$-^2P collision strength to be the strongest one, followed by the $^2P^o$-^2D and the $^2P^o$-^2S transitions. (An interesting feature is that the "resonance" transition $^2P^o$-^2D is weaker than a higher one.) A comparison is made with the experimental measurements for the cross section of the $^2P^o$-^2D transition and with other theoretical values.

The spin-forbidden transition $^2P^o$-^4P is of particular importance in astrophysical application, as the line intensity from the ^4P state is dependent on electron density. The line ratio $I(^2D\rightarrow{}^2P^o)/I(^4P\rightarrow{}^2P^o)$, for example, may be employed as a density diagnostic. A selected sample of the results for several transitions in the three ions is presented and described below.

A. $e+C^+$

With a relatively large number of excitation thresholds included in the scattering problem, the resonance structures become quite extensive as one has many interacting Rydberg series of autoionizing states converging on to the ion states in question. In order to delineate the resonances in detail we have carried out the calculations at a fine energy mesh ranging from the $2s2p^2(^4P)$ threshold to the highest $2p^3(^2P^o)$ threshold. The number of resonances thus obtained is too large to be able to identify all of them, however, a few of the most prominent, low-lying ones have been identified.

In Fig. 1 we plot the collision strength for the intercombination transition $^2P^o$-^4P. The transition has a significant amount of collision strength and although the background is not quite discernible, the resonances perhaps account for about 50% enhancement in the near-threshold region. The lowest resonances are identified as due to the state ^2D $3s$; however, slightly above this resonance the structures begin to overlap considerably and a precise identification becomes difficult. The irregularity in the overall collision strengths, in a resonance averaged sense, is an indication of the varying strengths of coupling to the various thresholds of excitation.

In Figs. 2(a)–2(c) we have plotted the collision strengths for the three optically allowed transitions $\Omega(^2P^o$-$^2D)$, $\Omega(^2P^o$-$^2S)$, and $\Omega(^2P^o$-$^2P)$. Although the resonance structures remain basically the same as in Fig. 1, the resonance enhancement relative to the background is less for the allowed transitions than for the forbidden ones. However, there is a strong feature at 0.82 Ry in $\Omega(^2P^o$-$^2D)$ that should make a significant effect on the collision strength in this region. As one might expect for the collision strengths of allowed transitions, the background rises with increasing energy for all three transitions. In an approximate manner one might estimate from Fig. 2 that $\Omega(^2P^o$-$^2D)$ is about 2.5 times larger than $\Omega(^2P^o$-$^2S)$ and about 30% smaller than $\Omega(^2P^o$-$^2P)$. These

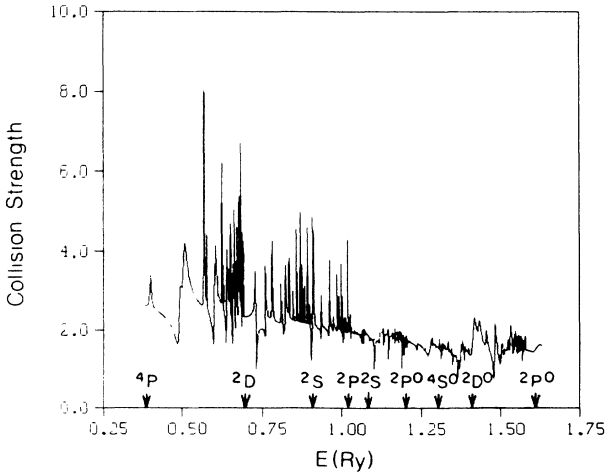

FIG. 1. Collision strength for the intercombination transition $^2P^o$-^4P in C^+.

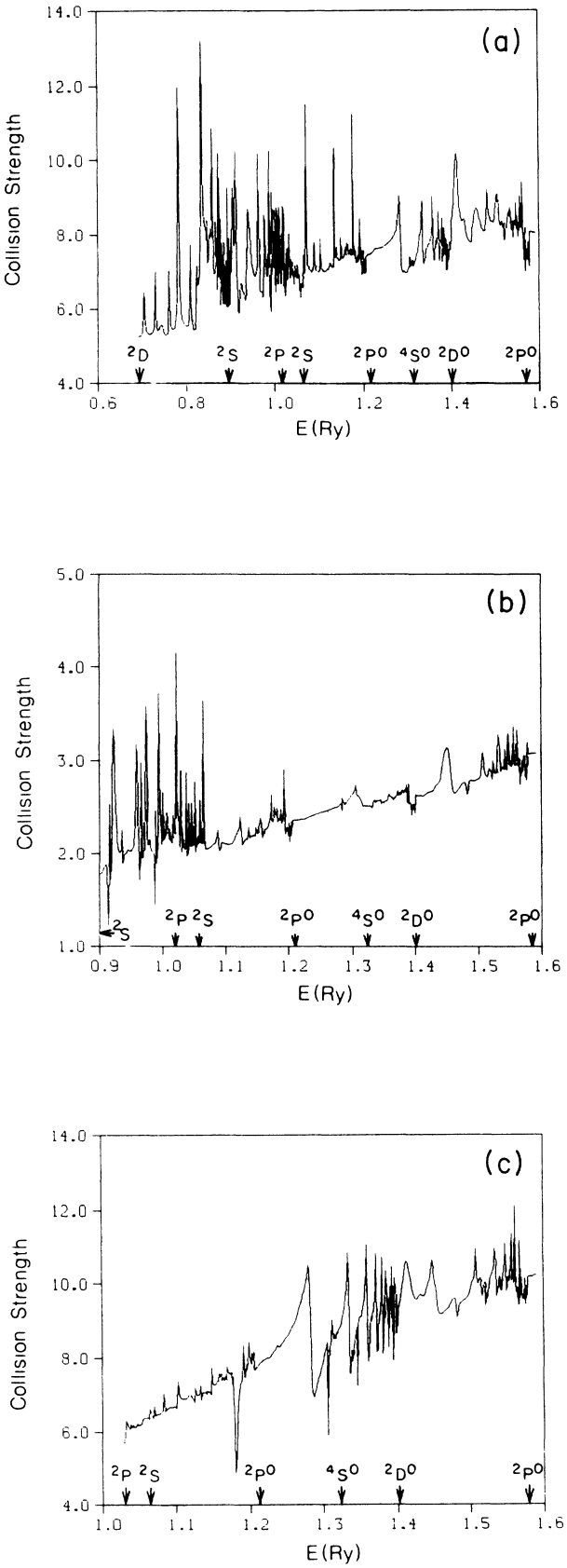

FIG. 2. Collision strengths for the allowed transitions (a) $^2P^o$-^2D; (b) $^2P^o$-^2S, and (c) $^2P^o$-^2P in C^+.

factors are not explained by simple calculations based on the Gaunt factor formula. The gf values for the ^2D, ^2S, and ^2P transitions from the ground state are 0.7487, 0.7752, and 3.1007, a proportion unrelated to the approximate proportion of the three collision strengths. It is clear that the coupling effects are rather strong and an accurate calculation can not be made without explicit consideration of the couplings and resulting resonance structures.

In Fig. 3 we have compared the cross section for the $^2P^o$-^2D transition with two sets of experimental data by Lafyatis and Kohl[10] and several theoretical calculations. The present theoretical curve appears to lie within the error bars of the experimental points (the first measured value is at an energy below threshold); however, the experimental uncertainties are rather large and a detailed comparison with the features in the theoretical results is precluded by the paucity of experimental data. For example, the large feature due to the cumulative effect of several resonances just below 12 eV is not covered by any experimental data point. Also, the experimental data do not extend into the higher energy region to determine the form of the cross section as it decreases with energy.

The two-state close-coupling calculations by Magee *et al.*[11] are shown by open squares in Fig. 3 and appear to lie about 20% above the background of the present results. The Coulomb-Born calculations by Magee *et al*,[11] with and without exchange, are also shown and are about a factor of two higher than the background cross sections from the present calculations (as expected, the weak cou-

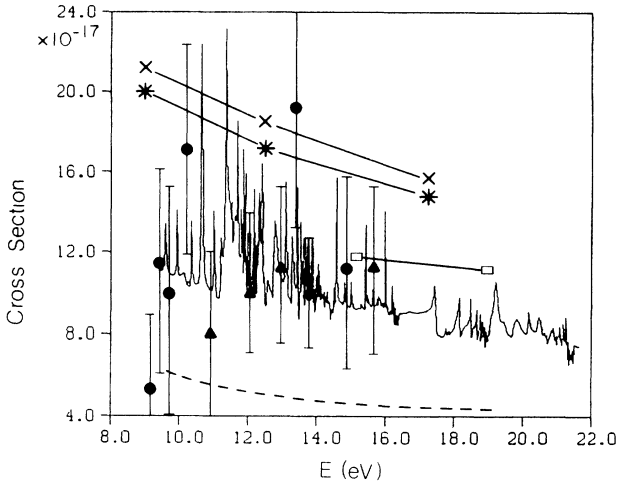

FIG. 3. Theoretical and experimental cross sections for the $^2P^o$-^2D transition: present (solid curve) and absolute measured cross sections (solid circles) and relative cross sections normalized to the point at 14.75 eV (solid triangles), both from Lafyatis and Kohl. Also shown are the two-state close-coupling values by Magee *et al.* (squares) and Coulomb-Born values with exchange by Magee *et al.* (asterisks) and without exchange (crosses), also by Magee *et al.* The Gaunt factor estimate is indicated by the dashed curve. The threshold cross-section value measured by Lafyatis and Kohl is $(1.1\pm0.3)\times10^{-16}$ cm^2, in nearly exact agreement with the present calculated value of 1.1×10^{-16} cm^2.

pling approximations tend to overestimate the cross sections as they do not allow for loss of flux into other open channels). Also for comparison we reproduce the Gaunt factor estimates given by Lafyatis and Kohl; the $\bar{g}$ formula (with $\bar{g}=0.2$) gives values that are approximately a factor of 2 lower than the present results, underscoring the point made above that the Gaunt factor formula, which is often used by astrophysicists, is not a reliable indicator of the actual cross sections even for resonance transitions.

A metastable state, due to its relatively longer lifetime, may be collisionally excited to higher levels, hence the dependence of its line intensity on electron density. In Fig. 4 we show the collision strength from the transition ^4P-$^4S^o$, the most likely transition for the upward excitation of the metastable ^4P state. As may be seen, the $\Omega(^4P$-$^4S^o)$ is quite large and much larger than the $\Omega(^2P^o$-$^4P)$. Based on these relative collision strengths one may be sure that the ^4P state stands a good chance of being quenched even in a moderately dense plasma.

The fine-structure transition between the substates of the ground state, $^2P^o_{1/2}$-$^2P_{3/2}$, is an important coolant in the interstellar region and the atmospheres of cool stars.[12] In Fig. 5 we present $\Omega(^2P^o_{1/2}$-$^2P^o_{3/2})$ with associated resonance structures. A few of the resonances shown could be identified according to their LS designation. The detailed collision strength is in good agreement with the previous close-coupling calculations by Hayes and Nussbaumer[13] (HN). The first resonance is in fact a doublet $2s2p^3(^1D^o, ^3D^o)$ and is at the same position as that of HN but differs somewhat in shape. The HN calculations were carried out in a five-state close-coupling (5CC) approximation, including the states $^2P^o$, ^4P, ^2D, ^2S, and ^2P. In addition to including twice as many states, the present calculations are at a much larger number of energies and therefore significantly more resonance structures are obtained. We employed the quantum-defect theory averaging procedure (Gailitis averaging) in the region just below the ^4P threshold. The resonance averaged values join smoothly with the resonance profile corresponding to the $2s2p^2(^2D)3s$ state just above the ^4P. As mentioned earlier, the resonance average is carried out only for the threshold of convergence in this case all resonances of the type $^4P\ nl$ are averaged over but resonance structures due to higher thresholds are retained, leading to a smooth continuation at the ^4P threshold.

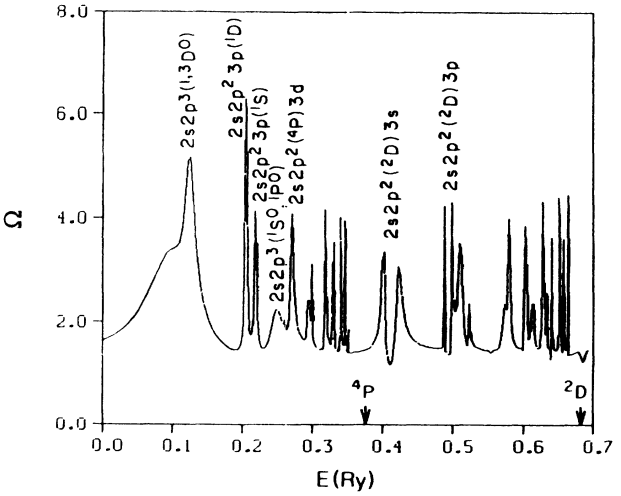

FIG. 5. Fine-structure collision strength for the transition $2s^22p(^2P^o_{1/2}$-$^2P^o_{3/2})$ in C^+.

Earlier calculations for electron-impact excitation of C^+ were also carried out by Lennon *et al.*[14] in an 8CC approximation, excluding the $2p^3$ states. They, as well as HN, have reported Maxwellian averaged collision strengths of transitions. A detailed comparison of rates with the present work, along with some astrophysical applications, will be given in a subsequent publication.

B. $e+N^{2+}$

The $n=3$ states $2s^23s$ and $2s^23p$ were excluded from the scattering calculations for N^{2+} and O^{3+}. Collision strengths were calculated for all remaining transitions at an energy mesh different from that for C^+ since the resonances get narrower with increasing ion charge.

In Fig. 6 we present the collision strength for the inter-

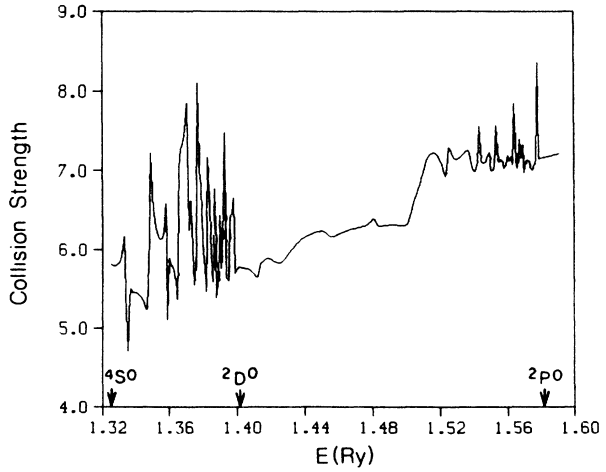

FIG. 4. Collision strength for the dipole allowed excitation of the metastable $2s2p^2(^4P)$ to $2p^3(^4S^o)$ in C^+.

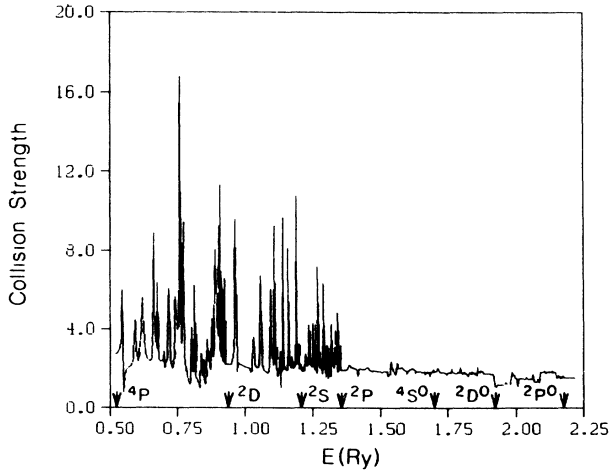

FIG. 6. Collision strength for the intercombination transition $^2P^o$-^4P in N^{2+}.

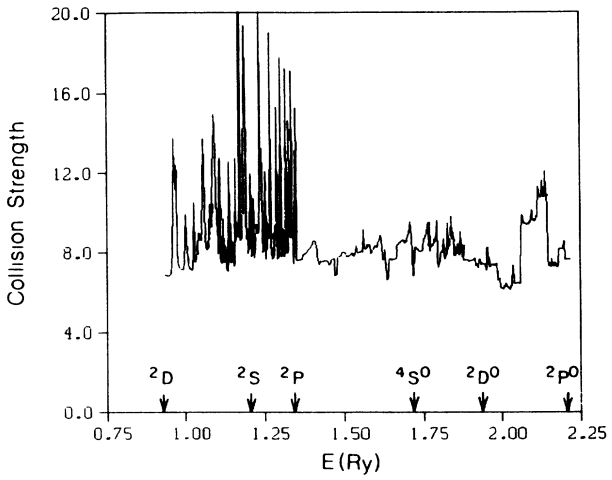

FIG. 7. Collision strength for the resonance transition $^2P^o$-^2D in N^{2+}.

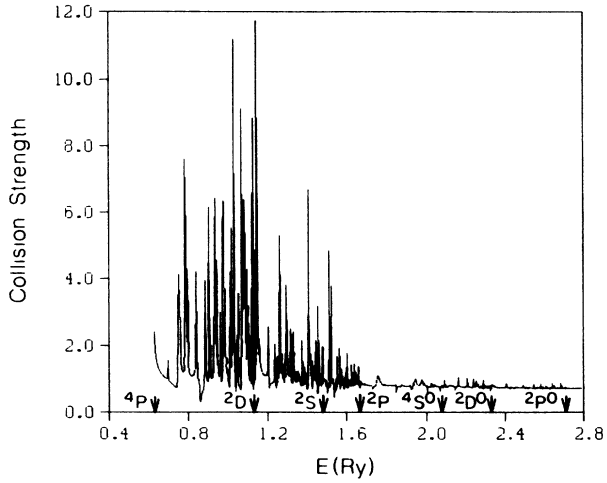

FIG. 9. Collision strength for the intercombination transition $^2P^o$-^4P in O^{3+}.

combination transition $^2P^o$-^4P. It is different from the corresponding one for C^+ (Fig. 1) in that the resonances are narrower and the background does not decrease appreciably over the energy range considered (the forbidden transitions become stronger with Z at a much faster rate than the allowed transitions).

Figure 7 shows the resonance transition in N^{2+}. Again comparing with Fig. 2(a) for C^+, we see narrower resonance structures but equally strong features in the near-threshold region, up to the $^4S^o$ threshold. There appears to be a rather large feature just above 2.0 Ry; however, it would not be accounted for by resonances converging on to the higher $^2P^o$ state since the coupling with the ground state, also $^2P^o$, is likely to be weak. It is perhaps a manifestation of the bound-channel pseudoresonances described in Sec. II. We shall discuss this further in Sec. V.

The collision strength for the fine-structure transition $\Omega(^2P^o_{1/2}$-$^2P^o_{3/2})$, is shown in Fig. 8. The prominent resonance doublet $2s2p^3(^1D^o,^3D^o)$ in Fig. 5 for C^+ is now a pure bound state for N^{2+}. The resonances due to the ^2D nl series could be identified unambiguously and are marked. The region just below the ^4P threshold contains a large resonance $2s2p^2(^2D)3d$ and it lies in the region of Gailitis averaging over the ^4P nl-type resonances. Similarly, just below the ^2D threshold we have a prominent feature due to a resonance belonging to the ^2P threshold $2s2p^2(^2P)3p$; again the resonances of the type ^2D nl have been averaged over, leaving the structures due to higher thresholds intact.

C. $e+O^{3+}$

$\Omega(^2P^o$-$^4P)$ is shown in Fig. 9 and appears to be similar to the corresponding ones for C^+ and N^{2+} except that the resonances are now very narrow. In particular, the resonances above the ^2P threshold are very weak and the background collisions strength can be clearly determined.

Figure 10 shows $\Omega(^2P^o$-$D)$ with a broad feature which is closer to the excitation threshold than for the other two ions. However, the effective resonance enhancement of this collision strength due to resonances is significantly

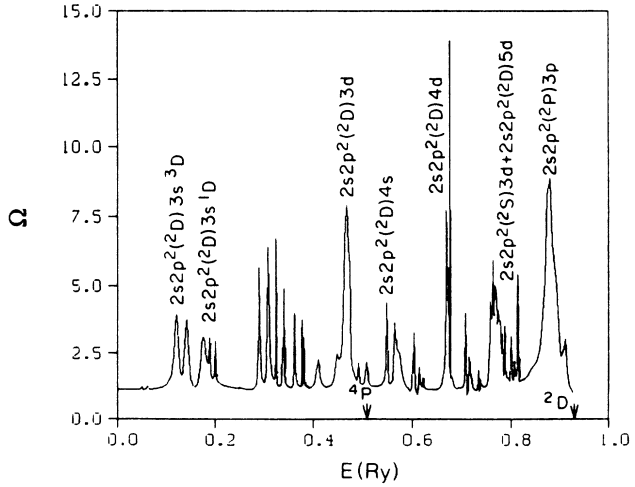

FIG. 8. Fine-structure collision strength for the transition $^2P^o_{1/2}$-$^2P^o_{3/2}$ in N^{2+}.

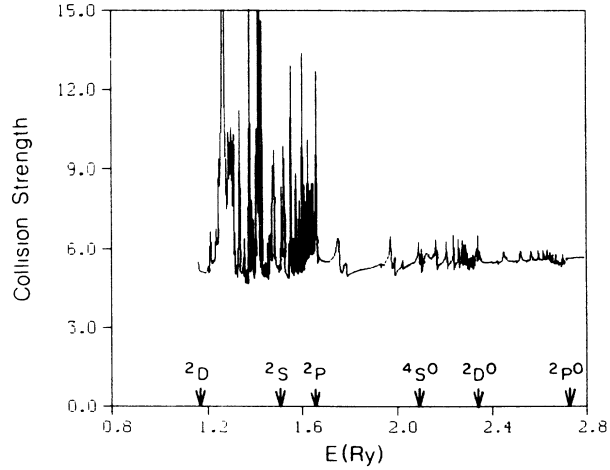

FIG. 10. Collision strength for the resonance transition $^2P^o$-^2D in O^{3+}.

less than for C^+. The overall values of $\Omega(^2P^o\text{-}^2D)$ and the $\Omega(^2P^o\text{-}^4P)$ appear to agree fairly closely with the five-state calculations by Hayes;[15] however, the detailed shapes of the resonance structures are not as well resolved as in the present work. A comparison of the present O^{3+} rate coefficients with the ones calculated by Hayes is in progress.

In Fig. 11 we show the fine-structure collision strength $\Omega(^2P^o_{1/2}\text{-}^2P^o_{3/2})$ which still shows some rather large resonance features. The resonances $2s2p^2(^2D)3s(^{1,3}D)$, obtained for N^{2+}, are now bound states, but the $(^2D)3d$ resonance, just above threshold, is quite prominent. It should be noted that most resonance states manifest themselves in a number of different $SL\pi$ states, with slightly different positions and shapes, and may add up to a large feature. For example, in the case of the $(^2D)3d$ resonance we expect contributions from total (electron + ion) symmetries with $L=0,1,2,3,4$ and $(2S+1)$ values of 1 and 3, a total of ten $SL\pi$ states of even parity. With increasing ion charge the energy separations also increase, broadening the resonance feature. At approximately 0.6 Ry we have the $2s2p^2(^2P)3p$ set of resonances in the Gailitis averaging region. It is found that this feature makes a noticeable contribution to the Maxwellian averaged effective collision strength even at temperatures slightly higher than 20 000 K.

V. BOUND-CHANNEL RESONANCES

The close-coupling method is a low-energy approximation for electron-ion collisions, usually employed for excitation of the few lowest levels of the target ion. As described in Sec. II, however, it is necessary to include a number of correlation functions in order to accurately represent the wave functions of the ion states in the eigenfunction expansion. In general, the larger the set of principal configurations, dominating the terms in the first sum of Eq. (1), the larger the set of bound correlation configurations in the second sum of Eq. (1). We therefore encounter a fundamental problem inherent in the close-coupling approximation. As one increases the number of principal ion states one needs to carry out the calculations at higher energies where the bound-channel eigenvalues, often constructed from nonspectroscopic pseudo-orbitals, are likely to be present, leading to pseudoresonances. The problem is also exacerbated if one attempts to improve the ion representation by including a large number of correlation configurations. To put it simply, one runs into these problems with the close-coupling method at intermediate energies. Thus, while present day supercomputers allow the inclusion of a large number of states, and solve the resulting coupled channel equations, many of the higher-lying eigenvalues and corresponding eigenfunctions are not obtained accurately.

In the present work, the eigenfunction expansion for C^+ is represented by a CI basis set that is approximately twice as large as the one for N^{2+} and O^{3+}. In addition, we have employed the $3d$ and the $n=4$ pseudo-orbitals $4s$, $4p$, and $4d$ in a scaled hydrogenic potential. In the $e+C^+$ scattering calculations we found large variations in the background collision strengths *above* all thresholds included in the eigenfunction expansion. While some of the bound-channel correlation eigenvalues also lie within the energy range covered by the C^+ thresholds, the wave functions in this energy range are predominantly determined by the continuum channel functions explicitly calculated in the R-matrix method and thus the effect of the bound channels is minimal in this region (i.e., the bound-channel functions simply provide additional correlation to the continuum channels).

In an effort to understand precisely the nature of the bound-channel resonances, we carried out an atomic structure calculation for neutral carbon employing the one-electron orbitals as obtained from the CI basis for C^+ (this is exactly the way in which the bound-channel

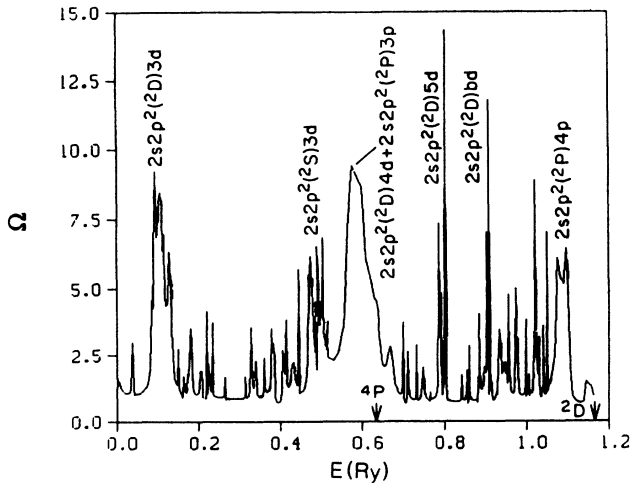

FIG. 11. Fine-structure collision strength for the transition $^2P^o_{1/2}\text{-}^2P^o_{3/2}$ in O^{3+}.

TABLE II. Some eigenvalues of bound-channel states of $e+C^+$ system.

State	Energy[a]
$2s2p^23p(^1P^o)$	1.5816
$2p^33p(^3S)$	1.6068
$2p^33p(^3D)$	1.6094
$2p^33d(^5D^o)$	1.6287
$2p^33p(^1P)$	1.6336
$2p^33s(^1P^o)$	1.6496
$2p^33p(^3P)$	1.6686
$2p^33p(^1D)$	1.6803
$2p^34d(^3D^o)$	1.7170
$2s^22p3d(D^o)$	1.7293
$2s^22p3d(^3P^o)$	1.7554
$2s^22p3d(^3D^o)$	1.8140
$2p^33d(^3F^o)$	1.8303
$2p^33d(^1S^o)$	1.8314
$2p^33d(^3G^o)$	1.8461
$2p^33d(^1G^o)$	1.8634
$2p^33d(^1P^o)$	1.8734
$2p^33p(^1S)$	1.8968
$2p^34d(^1F^o)$	1.9035

[a]Relative to the ground state $2s^22p\ ^2P^o$ of C^+. All energies are in rydbergs.

functions are constructed in the close-coupling formulation). The CI basis for C^0 is then chosen to consist of the configurations determined by the $e+C^+$ system, given the C^+ states that have been included. The atomic structure calculation for C^0 yields a large number of states; in the present problem we determined 156 states lying *above* the highest threshold of C^+ ($2p^3\,^2P^o$). In Table II we have given a few of these eigenvalues. It is therefore not surprising that the collision strengths for $e+C^+$ scattering, in the region above all thresholds, contain structures due to the large number of bound channels present.

The problem may be circumvented in one of the following two ways: (i) a $\underline{T}$-matrix averaging procedure described by Burke, Berrington, and Sukumar;[16] or (ii) carrying out the $\underline{R}$-matrix calculations with a simpler target ion represented by very few configurations. Method (i) essentially entails the determination of a background $\underline{T}$ matrix that includes in an average sense the rapid variations due to the bound channels. However, in practice it may be difficult to employ this procedure, particularly when a large number of bound channels are present. At present we are using method (ii) to calculate the collision strengths in the intermediate energy region with all channels open. Different basis sets for C^+, necessarily small, are employed in the calculation to achieve reasonable agreement with the full 10CC calculations at the highest threshold $2p^3\,^2P^o$. The calculation of the rate coefficients at high temperatures requires the collision strengths at high energies, which would be obtained through the simpler calculation. For N^{2+} and O^{3+}, the problem of pseudoresonances at high energies will also be considered in the same manner.

VI. SUMMARY

$\underline{R}$-matrix calculations are reported for a large number of transitions in C^+, N^{2+}, and O^{3+} due to electron impact. An extended $\underline{R}$-matrix package, recently developed for the Opacity Project, is employed for the close-coupling calculations. Fine-structure transitions have been considered through an algebraic transformation of the *LS* coupled reactance matrices to a pair-coupling formulation. The problem of bound-channel resonances in the close-coupling method in the intermediate to high-energy range is discussed and calculations are under way to obviate the problem. The calculation of rate coefficients at representative temperatures for the presence of C^+, N^{2+}, and O^{3+} in astrophysical and laboratory plasmas will be undertaken subsequently. The dataset with the detailed collision strengths may be obtained from one of the authors (A.K.P.).

ACKNOWLEDGMENTS

This work was supported by an astrophysical theory grant from NASA, Grant No. NAGW 766, for D.L.; and by a grant from the U.S. Department of Energy, Office of Fusion Energy, for A.K.P.

---

*Present address: Department of Astronomy, Ohio State University, Columbus, OH 43210-1106.

[1]K. A. Berrington, P. G. Burke, K. Butler, M. J. Seaton, P. J. Storey, K. T. Taylor, and Y. Yu, J. Phys. B **20**, 6379 (1987).
[2]M. J. Seaton, J. Phys. B **20**, 6363 (1987).
[3]H. E. Saraph, Comput. Phys. Commun. **15**, 247 (1978); **3**, 256 (1972).
[4]M. J. Seaton, J. Phys. B **2**, 5 (1969).
[5]A. K. Pradhan, Mon. Not. R. Astron. Soc. **177**, 31 (1976).
[6]D. Luo and A. K. Pradhan, J. Phys. B (to be published).
[7]A. Burgess and V. B. Storey, J. Phys. B **7**, 2403 (1974).
[8]A. K. Pradhan, Phys. Rev. A **28**, 2113 (1983).
[9]V. M. Burke and M. J. Seaton, J. Phys. B **19**, L527 (1986).
[10]G. P. Lafyatis and J. L. Kohl, Phys. Rev. A **36**, 59 (1987).
[11]N. H. Magee, J. B. Mann, A. L. Merts, and W. D. Robb, Los Alamos Report No. LA-6691-MS (1977).
[12]D. E. Osterbrock, *Astrophysics of Gaseous Nebulae and Active Galactic Nuclei* (University Science Books, 1989).
[13]M. A. Hayes and H. Nussbaumer, Astron. Astrophys. **134**, 193 (1984).
[14]D. J. Lennon, P. L. Dufton, A. Hibbert, and A. K. Kingston, Astrophys. J. **294**, 200 (1985).
[15]M. Hayes, J. Phys. B **16**, 285 (1983).
[16]P. G. Burke, K. A. Berrington, and C. V. Sukumar, J. Phys. B **16**, 2553 (1983).